Sensors & Actuators: B. Chemical 323 (2020) 128702

Contents lists available at ScienceDirect

Sensors and Actuators: B. Chemical

journal homepage: www.elsevier.com/locate/snb

Signal-off electrochemiluminescence immunosensor based on Mn-Eumelanin coordination nanoparticles quenching PtCo-$CuFe_2O_4$-reduced graphene oxide enhanced luminol

Xiaojian Li [a], Yu Du [a], Peng Xu [a], Yueyun Li [b], Xiang Ren [a], Hongmin Ma [a], Huan Wang [a,*], Qin Wei [a,*], Huangxian Ju [a,c]

[a] Collaborative Innovation Center for Green Chemical Manufacturing and Accurate Detection, Key Laboratory of Chemical Sensing & Analysis in Universities of Shandong, School of Chemistry and Chemical Engineering, University of Jinan, Jinan, 250022, PR China
[b] School of Chemical Engineering, Shandong University of Technology, Zibo, 255049, PR China
[c] State Key Laboratory of Analytical Chemistry for Life Science, School of Chemistry and Chemical Engineering, Nanjing University, Nanjing, 210023, PR China

ARTICLE INFO

Keywords:
Manganese-eumelanin coordination nanocomposites
PtCo bimetallic
$CuFe_2O_4$ nanoparticles
Electrooxidation of luminol and H_2O_2
Quench
Electrochemiluminescence

ABSTRACT

Herein, a facile one-pot intrapolymerization strategy to synthesize manganese-eumelanin coordination nanocomposites (Mn-Eu) was introduced to quench the electrochemiluminescence (ECL) behavior of luminol/H_2O_2 system. Bimetallic PtCo and $CuFe_2O_4$ nanoparticles decorated with reduced graphene oxide was prepared to combine with luminol via electrostatic attractions (Lu-PtCo-$CuFe_2O_4$-rGO) which possessed excellent ECL signals. PtCo-$CuFe_2O_4$-rGO not only exhibited well electrocatalytic activity toward the electrooxidation reactions of luminol and H_2O_2, but also facilitated the electroreduction of H_2O_2 producing more reactive oxygen species (ROSs) which can further enhance the ECL intensity of luminol. To sensitively detect procalcitonin, Mn-Eu labeled-secondary antibodies were employed to specific recognize antigen which incubated with primary antibodies/Lu-PtCo-$CuFe_2O_4$-rGO. The quenching mechanism may be via the synergistic effect between Mn-Eu inhibiting the electrooxidation of H_2O_2 and ECL resonance energy transfer (ECL-RET) from ECL donor luminol to ECL acceptor Mn-Eu. Under optimal experiments, the ECL immunosensor for detecting procalcitonin with a wider linear range from 0.005 pg/mL to 100 pg/mL and a detection limit of 0.0021 pg/mL (S/N = 3) was obtained. The suggested strategy possessed great potential in bioanalysis and will broaden the application of Mn-Eu.

1. Introduction

Electrochemiluminescence (ECL) technique has been extensively employed in bioanalysis field, with combining the advantages of electrochemistry and chemiluminescence, such as high sensitivity, rapid responses and wide detecting range [1,2]. Under suitable potential, the excited substances would generate energy relaxation process with emitting light at the surface of electrode, thus ECL is considered as photoemission behavior [3]. Recently, the method of immobilizing luminol on nanomaterials' surface has been widely researched and luminol as classical luminophore, exhibited excellent luminous efficiency in aqueous solution [4]. However, lower luminous efficiency of luminol on most nanomaterials is still a challenge. To improve this problem, nanomaterials with excellent conductivity and catalytic properties toward coreactant H_2O_2 have been widely used to combine with luminol [5]. As to our knowledge, magnetic spinel-structured copper ferrite ($CuFe_2O_4$), holding excellent chemical stability and well catalytic activity, has extensively attracted in the degradation of various organic hazards and the purification of wastewater [6–8]. Nevertheless, high agglomeration of pure $CuFe_2O_4$ could restrain its application in bioanalysis field [9]. To improve the insufficiency, graphene oxide (GO) was employed as support materials to disperse $CuFe_2O_4$ nanoparticles in this work. During preparation process, GO could be reduced by ethylene glycol forming reduced GO (rGO), and then rGO has offered a conductive backbone to facilitate electron transport, as an attracting two-dimensional carbon material [10]. The hybrid materials ($CuFe_2O_4$-rGO) can improve electrochemical performance with the synergistic effect between rGO and transition metal oxides. To further

* Corresponding authors.
E-mail addresses: wanghuan8711@163.com (H. Wang), sdjndxwq@163.com (Q. Wei).

https://doi.org/10.1016/j.snb.2020.128702
Received 21 May 2020; Received in revised form 22 July 2020; Accepted 2 August 2020
Available online 5 August 2020

enhance the catalytic effect of hybrid materials towards H_2O_2, PtCo bimetallic nanoparticles could be in situ anchored on the surface of $CuFe_2O_4$-rGO. Pt nanoparticles could accelerate the decomposition of H_2O_2 generating reactive oxidize species which can react with luminol radical anion emitting light [11]. Moreover, Co nanoparticles could catalyze the electrochemical oxidation of luminol and hydrogen peroxide [12]. Therefore, the integration of PtCo bimetallic nanoparticles and $CuFe_2O_4$-rGO could enable the ECL behavior of luminol/H_2O_2 system more excellent.

Procalcitonin is a protein consisting of 116-amino-acids with a molecular weight of 13 kDa [13,14]. The concentrations of PCT in the blood of a healthy person is below 0.1 ng mL^{-1} and it can increase over 100 ng mL^{-1} for the bacteria originated sepsis, depending on the severity of the infection [15,16]. To sensitively detect biomarker procalcitonin for monitoring bacterial infections, a quenching sandwich immunosensor was proposed based on manganese-eumelanin coordination nanoparticles (Mn-Eu) quenching the ECL of PtCo-$CuFe_2O_4$-rGO combined luminol. Eumelanin is a part of melanin and also the black insoluble photoprotective pigments of human skin and eyes [17]. The structure of eumelanin cannot be described accurately beyond a statistical description of main units and functional groups [17]. This could be primarily because of the amorphous character, the marked insolubility in all solvents, and the close association with the cellular ingredients of the biological matrix [17]. Thus far, however, some paramagnetic metal ions including Fe, Gd, and Mn, have been employed to react with melanin which possessing the ability of chelating with metal ions synthesizing melanin-like nanoparticles [18–20]. Moreover, these prepared hybrid nanomaterials exhibited a broadband UV–vis absorption [21], an intrinsic free radical character [22], efficient nonradiative energy dissipation [23], and a water-dependent, ioni c-e lectronic hybrid conductor behavior [24]. Herein, Mn-Eu were synthesized via chemical oxidation-polymerization of 3,4-dihydroxy-DL-phenylalanine (DL-DOPA) in the presence of $KMnO_4$ which can oxidize DL-DOPA and provide Mn source. During the process of preparing, the catechol group of DL-DOPA may be oxidized by $KMnO_4$ forming benzoquinone group, intramolecular cyclization through Michael reaction to generate indole, polymerization to eumelanin, and Mn chelation [25]. The prepared Mn-Eu with excellent solubility can effectively decrease the ECL intensity of luminol/H_2O_2 system which may be due to inhibiting the electrooxidation of H_2O_2 and ECL resonance energy transfer (ECL-RET) between Mn-Eu and luminol.

2. Experimental section

2.1. Preparation of PtCo-$CuFe_2O_4$-rGO

Graphene oxide was prepared through Hummer method and the detailing process was provided in Supplementary Material. $CuFe_2O_4$-rGO was prepared according to previous literature with a slight modification [26]. Firstly, 0.5 g BSA was dispersed in 5 mL ultrapure water, following by 50 mg GO ultrasonic dispersion 1 h in the ultrapure water. Then, 25 mL ethylene glycol was added in BSA solutions. After vigorous stirring for 5 min, 0.17 g $CuCl_2{\cdot}2H_2O$, 0.54 g $FeCl_3{\cdot}6H_2O$ and 0.75 g NaAc were successively dispersed into the mixture solutions under stirring for 2 h. Finally, the mixture solutions were transferred into a Teflon-lined autoclave and heated at 180 °C for 24 h. After removing unreacted impurities by centrifugation and water washing, the prepared $CuFe_2O_4$-rGO was freeze dried.

20 mg $CuFe_2O_4$-rGO was added in 15 mL ethylene glycol under ultrasounding for 30 min. 45 mg L-proline was dissolved in the above solutions under mechanical stirring. After 100 μL $H_2PtCl_6{\cdot}6H_2O$ and 7 mg $CoCl_2$ $6H_2O$ added, the mixture solutions were transferred to a Teflon-lined autoclave and heated at 180 °C for 12 h. The products were washed several times using ultrapure water and absolute ethyl alcohol to remove unreacted impurities, then freeze drying.

The Zeta-potential of PtCo-$CuFe_2O_4$-rGO was 6.6 mV, but the Zeta-potential of luminol was −8.14 mV. Thus, luminol can adsorb on the surface of PtCo-$CuFe_2O_4$-rGO through electrostatic attraction. In brief, 1 mL 5 mM luminol was diluted to 10 mL and 10 mg PtCo-$CuFe_2O_4$-rGO was dispersed in the diluted solutions under oscillating 6 h. After centrifugal washing, obtained Lu-PtCo-$CuFe_2O_4$-rGO was dispersed in 1 mL 0.5 % chitosan.

2.2. Preparation of Mn-Eu-Ab_2

Synthesis of Mn-Eu was performed by chemical oxidation-polymerization of DL-DOPA with $KMnO_4$ in aqueous solution [25]. Briefly, 0.118 g DL-DOPA was added in 60 mL ultrapure water and heated to 50 °C. Following by, 0.01 g PVP was dissolved in the above solution. 1.8 mL 100 mM $KMnO_4$ solution was rapidly dropped under vigorous stirring. After continuous stirring for 6 h, the black products were collected by centrifugation (15,000 rpm, 10 min) and washing with ultrapure water three times. Finally, the precipitate was freeze dried.

According to the -COOH of Mn-Eu, second antibodies were immobilized on the surface of Mn-Eu through covalent linkage. In brief, 3 mg Mn-Eu was dispersed in pH 7.4 PBS. After 500 μL 100 mM EDC and 500 μL 400 mM NHS added in the PBS, 500 μL 100 μg/mL Ab_2 was dropped. After oscillating 6 h at 4 °C, Mn-Eu-Ab_2 immune complex was obtained by centrifugation and washing with ultrapure water and redispersed in pH 7.4 PBS. To block non-specific sites, 300 μL 1% BSA was dropped in the Mn-Eu-Ab_2 immune complex solutions under oscillating 6 h at 4 °C. The immune complex was redispersed in pH 7.4 PBS and stored at 4 °C.

2.3. Fabrication and detection procedure of ECL immunosensor

The pretreatment process of ITO was according to our previous work. Scheme 1 represented the assembly process of ECL immunosensor and its application of detecting procalcitonin. First, ITO was modified with 6 μL of Lu-PtCo-$CuFe_2O_4$-rGO chitosan solution and dried. Subsequently, Ab_1 was incubated with the modified electrode. The Zeta-potential of Lu-PtCo-$CuFe_2O_4$-rGO chitosan solution was 60.5 mV due to electropositive chitosan and the Zeta-potential of Ab_1 was -9.02 mV. Thus, Ab_1 can adsorb on the surface of Lu-PtCo-$CuFe_2O_4$-rGO chitosan solution through electrostatic attraction. After being rinsed with ultrapure water, the modified electrode was blocked with 3 μL of 1% BSA. After incubating 30 min, the modified electrode was rinsed and 6 μL of different concentrations of procalcitonin was dropped and incubated at 4 °C for 1 h. After rinsed, 6 μL of 2 mg/mL Mn-Eu-Ab_2 was incubated with procalcitonin/BSA/Ab_1/PtCo-$CuFe_2O_4$-rGO-modified ITO for 1 h to form Mn-Eu-Ab_2/procalcitonin/BSA/Ab_1/PtCo-$CuFe_2O_4$-rGO-ITO.

The fabricated ECL immunosensor was detected in 10 mL pH 8.0 PBS containing 6 mM H_2O_2. The voltage of the photomultiplier tube at 800 V and the potential from 0 to 0.6 V were carried out to detect the ECL signals of the fabricated ECL immunosensor.

3. Results and discussion

3.1. Characterization of the synthesized $CuFe_2O_4$-rGO, PtCo-$CuFe_2O_4$-rGO and Mn-Eu

The morphology of $CuFe_2O_4$-rGO and PtCo-$CuFe_2O_4$-rGO was characterized by SEM. As shown in Fig. 1A, $CuFe_2O_4$ was uniformly distributed on the rGO surface. The large surface of GO was rich in defects/functional groups as nucleation sites and the feature of GO can make in-situ growth of $CuFe_2O_4$ nanoparticles avoid agglomeration. The solvent EG served as weak reductants to reduce obtaining reduced graphene oxide (rGO) and BSA was employed as surfactant to improve the biocompatibility of $CuFe_2O_4$-rGO. The prepared GO exhibited flake-like shaped (Fig. S1 in Supplementary Material). The morphology of the pure $CuFe_2O_4$ aggregated each other creating clumps without adding GO

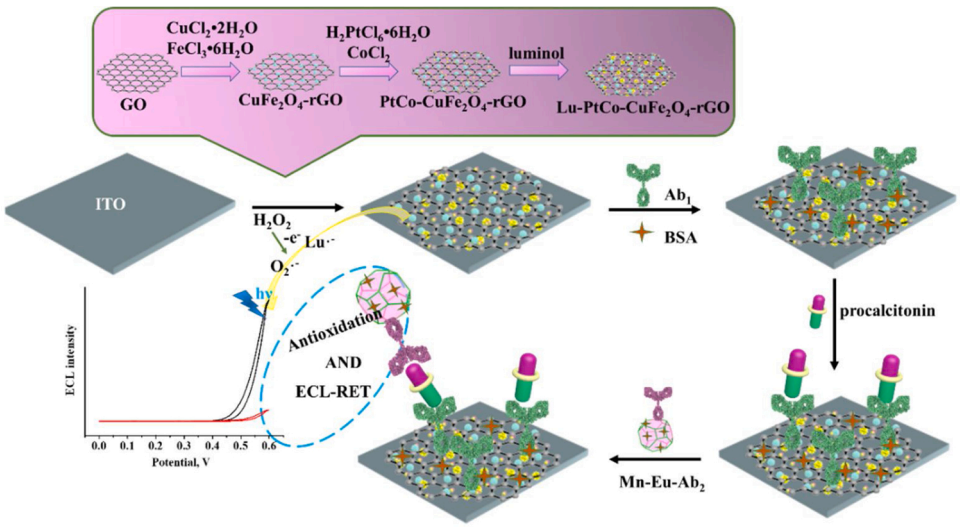

Scheme 1. Schematic illustration of constructed process of the developed signal-off ECL immunosensor for detecting procalcitonin.

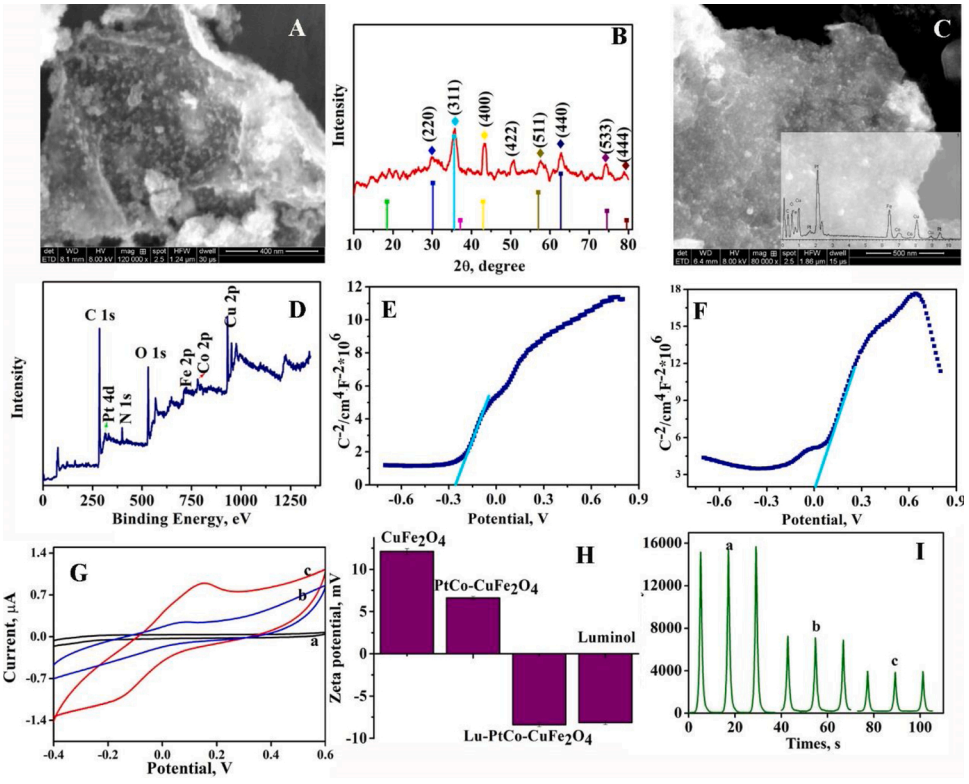

Fig. 1. SEM images of $CuFe_2O_4$-rGO (A) and PtCo-$CuFe_2O_4$-rGO (C); XRD pattern of $CuFe_2O_4$-rGO (B); XPS survey spectrum of PtCo-$CuFe_2O_4$-rGO (D); Mott-Schottky plots of $CuFe_2O_4$-rGO (E) and PtCo-$CuFe_2O_4$-rGO (F) in 0.2 M Na_2SO_4 and the frequency was 2000 Hz; (G) CV of bare ITO (curve a), $CuFe_2O_4$-rGO (curve b) and PtCo-$CuFe_2O_4$-rGO (curve c) in pH 8.0 PBS containing 6 mM H_2O_2; (H) Zeta-potential of $CuFe_2O_4$-rGO, PtCo-$CuFe_2O_4$-rGO, luminol and Lu-PtCo-$CuFe_2O_4$-rGO; (I) ECL behavior of Lu-PtCo-$CuFe_2O_4$-rGO (curve a), Lu-Pt-$CuFe_2O_4$-rGO (curve b) and Lu-Co-$CuFe_2O_4$-rGO (curve c) in pH 8.0 PBS containing 6 mM H_2O_2. Error bars = RSD (n = 3).

(Fig. S2 in Supplementary Material). Besides, XRD was used to characterize the crystal structure of $CuFe_2O_4$-rGO (Fig. 1B). Diffraction peaks were exhibited at 29.8° (220), 35.64° (311), 43.03° (400), 57.64° (511), 62.77° (440), 74.24° (533) and 78.96° (444), which agreed well with the standard XRD data for Cuprospinel $CuFe_2O_4$ (JCPDS NO. 25-0283). Fig. 1C showed the SEM of PtCo-$CuFe_2O_4$-rGO and large nanoparticles including PtCo and $CuFe_2O_4$ nanoparticles were observed on the rGO surface. The inset of Fig. 1C was the EDX of PtCo-$CuFe_2O_4$-rGO and the main elements were displayed containing Pt, Co, Cu, Fe, O and C, confirming the chemical composition of PtCo-$CuFe_2O_4$-rGO. The chemical state of element exhibited in the PtCo-$CuFe_2O_4$-rGO was characterized by XPS. Fig. 1D was the survey spectrum of PtCo-$CuFe_2O_4$-rGO, confirming the existence of Pt, Co, Cu, Fe, O and C elements which was consistent with EDX of PtCo-$CuFe_2O_4$-rGO. For Pt nanoparticles, the strong peaks at 70.2 eV and 73.5 eV were fitted with Pt° $4f_{7/2}$ and Pt° $4f_{5/2}$, then the peak centered at 76.0 eV was corresponding to Pt^{2+} (Fig. S3A) [27]. As shown in Fig. S3B, the binding energies of Co $2p_{3/2}$ and Co $2p_{1/2}$ were located at 780.4 eV and 796.4 eV, while the weaker peak at 784.5 eV belonging to Co^{2+} [28]. Fig. S3C–F was the high-resolution spectra of Cu, Fe, O and C elements, and the peaks for Cu $2p_{3/2}$ at 931.3 eV, Cu $2p_{1/2}$ at 951.2 eV, Cu^{2+} at 943.3 eV, Fe $2p_{3/2}$ at 711.4 eV, O 1s at 530.5 eV, C—C at 283.7 eV, C—O at 284.9 eV and C═O at 287.1 eV can be shown clearly, forming the components of $CuFe_2O_4$-rGO. Herein, PtCo-$CuFe_2O_4$-rGO exhibited more excellent catalytic activity towards luminol/H_2O_2 system than $CuFe_2O_4$-rGO. Mott-Schottky plots measurement was performed to investigate the

catalytic performance. As Fig. 1E and F presented, the Fermi levels of $CuFe_2O_4$-rGO and PtCo-$CuFe_2O_4$-rGO were about -0.26 V and 0.01 V, respectively. The results indicated that the Femi energy decreased after PtCo nanoparticles grown on the $CuFe_2O_4$-rGO surface, thus PtCo-$CuFe_2O_4$-rGO much more easily received electrons from luminol to H_2O_2 promoting the decomposition of H_2O_2 to produce more ROS which can enhance the ECL of luminol. Moreover, cyclic voltammetry (CV) of bare ITO (curve a, Fig. 1G), $CuFe_2O_4$-rGO (curve b, Fig. 1G) and PtCo-$CuFe_2O_4$-rGO (curve c, Fig. 1G) was carried out in pH 8.0 PBS containing 8 mM H_2O_2. The CV of PtCo-$CuFe_2O_4$-rGO presented obvious reductive peak at −0.15 V compared to $CuFe_2O_4$-rGO, indicating that PtCo-$CuFe_2O_4$-rGO as mimicking peroxidase-like much more easily facilitate the decomposition of H_2O_2 producing more ROS. The immobilizing method of luminol on nanomaterials' surface was related to the stable of ECL signals. As shown in Fig. 1H, the Zeta-potential of $CuFe_2O_4$-rGO and PtCo-$CuFe_2O_4$-rGO was 12.1 mV and 6.6 mV, respectively. However, the Zeta-potential of luminol was −8.14 mV. Therefore, luminol can immobilize on the surface of PtCo-$CuFe_2O_4$-rGO through electrostatic attraction. The Zeta-potential of Lu-PtCo-$CuFe_2O_4$-rGO was −8.39 mV, indicating that luminol was successfully anchored on the PtCo-$CuFe_2O_4$-rGO surface.

The morphology of Mn-Eu was characterized by TEM which presented a sphere-like structure. As shown in Fig. S4E, Dynamic Light Scattering (DLS) was employed to characterize the size of Mn-Eu, and DLS results showed that the average size was about 138 nm which was consistent with the TEM measured. XPS was performed to analyze the chemical state of the elements in Mn-Eu. Fig. S4A was the survey spectrum of Mn-Eu, confirming the existence of C, N, O and Mn elements. Fig. S4B and C were the spectra of N 1s and O 1s, displaying the characteristic peak was centered at 399.4 eV and 530.9 eV, respectively. Fig. 2B was the Mn 2p spectra and showed two characteristic peaks located at 641.2 eV and 653.1 eV, belonging to Mn $2p_{3/2}$ and Mn $2p_{1/2}$, respectively, demonstrating the presence of Mn^{2+}. The weak peak at 645.6 eV can reveal the existence of Mn^{3+}. Fig. 2C was the spectra of C 1s and the binding energies centered at 284.2 eV, 285.1 eV and 287.3 eV were assigned to C—C, C—O and C═O, respectively, suggesting that the presence of −COOH in Mn-Eu. To further confirm the presence of −COOH in Mn-Eu, as presented in Fig. S4D, FT-IR was carried out and the peaks at 1629 cm^{-1} and 1400 cm^{-1} were assigned to C═O and C—O stretching, respectively [29]. In my view, the source of the −COOH in Mn-Eu was DL-DOPA. Therefore, EDC/NHS was employed to activate the −COOH of Mn-Eu attaching antibodies. As shown in Fig. 2D, the Zeta-potential of Mn-Eu and Ab_2 was −17.6 mV and −9.02 mV, respectively. After Ab_2 attached, the Zeta-potential was −35.3 mV, indicating Ab_2 was successfully anchored on the Mn-Eu surface.

3.2. Possible ECL reaction mechanism of Mn-Eu quenching Lu-PtCo-$CuFe_2O_4$-rGO/H_2O_2 system

The ECL mechanism of luminol/H_2O_2 system was based on the electrochemical oxidation-reduction reaction of luminol and H_2O_2. First, under positive potential, deprotonation of luminol in an alkaline solution (pH 8.0) was electrochemical oxidized forming radical anions of 3-aminophthalic acid. While H_2O_2 was under the potential scanning from 0 V to 0.6 V, it could be electrooxidation forming superoxide radical anions. Then, radical anions of 3-aminophthalic acid could be oxidized by superoxide radical forming excited anions of 3-aminophthalic acid which can emit light. As shown in Fig. 1G, PtCo-$CuFe_2O_4$-rGO not only increased the electrooxidation current of H_2O_2, but also catalyzed the decomposition of H_2O_2 producing more ROSs. To investigate the vital role of adding PtCo nanoparticles, pure Pt nanoparticles and pure Co nanoparticles were also prepared to electrostatic attract the same concentration of luminol. The ECL-time curve of Lu-PtCo-$CuFe_2O_4$-rGO/ITO (curve a in Fig. 1I), Lu-Pt-$CuFe_2O_4$-rGO/ITO (curve b in Fig. 1I) and Lu-Co-$CuFe_2O_4$-rGO/ITO (curve c in Fig. 1I) was performed in pH 8.0 PBS containing 6 mM H_2O_2, revealing that only Pt nanoparticles and Co nanoparticles co-existence, the PtCo-$CuFe_2O_4$-rGO/ITO exhibited optimal ECL behavior. We can deduce that PtCo

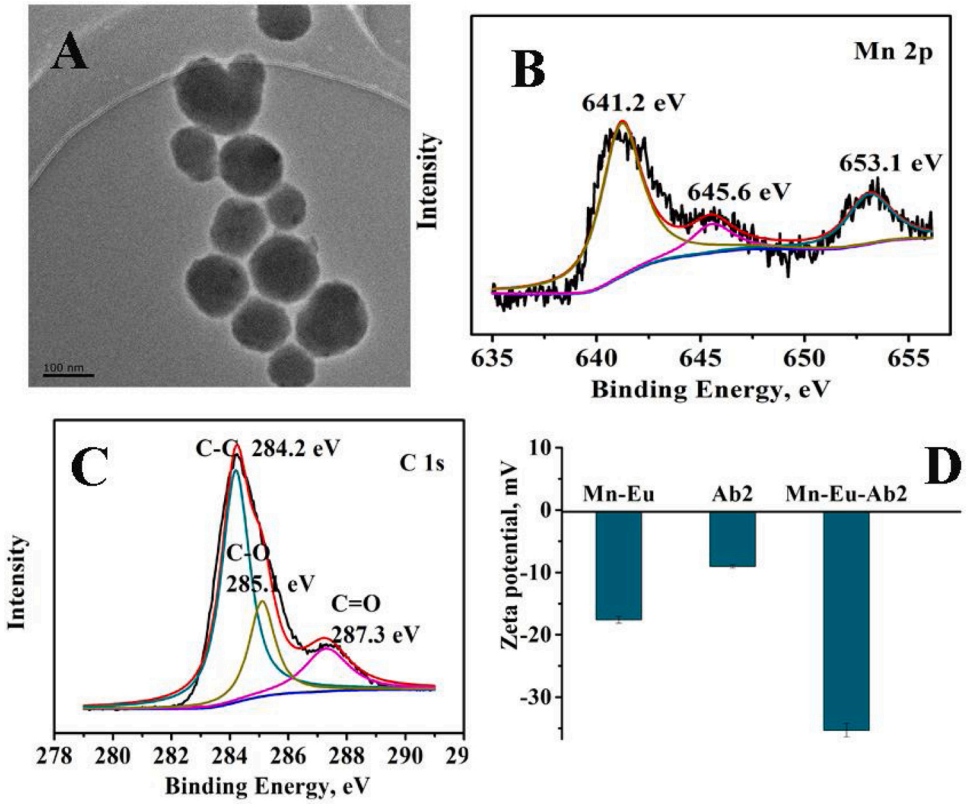

Fig. 2. TEM image of Mn-Eu (A); XPS spectra of Mn 2p (B) and C 1s (C); Zeta-potential of Mn-Eu, Ab_2 and Mn-Eu-Ab_2 (D). Error bars = RSD (n = 3).

nanoparticles possess better catalytic activity than pure Pt and Co nanoparticles.

As depicted in Fig. 4A, Lu-PtCo-$CuFe_2O_4$-rGO modified-ITO exhibited strong ECL signal (curve a), but the ECL intensity decreased sharply after Mn-Eu casted on the Lu-PtCo-$CuFe_2O_4$-rGO modified-ITO (curve b). The ECL reaction was occurred at the electrode surface. To investigate the quenching mechanism, CV performance of Mn-Eu in the absence or presence of H_2O_2 was conducted and bare glass carbon electrode was used as working electrode. As shown in Fig. 3A, curve a and b were the CV of bare GCE in the absence and presence of 10 μM H_2O_2, respectively. The oxidation current of bare GCE at 10 μM H_2O_2 obviously increased which was ascribed to the electrooxidation of H_2O_2. To investigate the effect of Mn-Eu on the electrode surface, the CV of Mn-Eu modified GCE was performed in the absence (curve c) and presence (curve d) of 10 μM H_2O_2. It was found that the current intensity was no distinct change before and after adding H_2O_2, indicating that Mn-Eu maybe inhibit the electrooxidation of H_2O_2 producing less superoxide radical anions. As we all know, superoxide radical anions can react with radical anions of 3-aminophthalic acid producing excited anions of 3-aminophthalic acid. Therefore, the existence of Mn-Eu can be used as antioxidant to quench the ECL behavior of luminol/H_2O_2 system. Besides, the ECL emission of luminol was investigated and the result was shown in Fig. 3B curve a. It was found that emission rang was from 365 nm to 600 nm and the characteristic peak was at about 438 nm. The UV–vis absorbance spectrum of Mn-Eu was displayed in Fig. 3B curve b. The absorbance range was from 260 nm to 800 nm and the characteristic peak was located at 312 nm. Combination curve a and curve b, partial overlap between the ECL emission spectrum of luminol and UV–vis absorbance spectrum of Mn-Eu was revealed, indicating that the presence of ECL resonance energy transfer (ECL-RET) from ECL donor luminol to ECL acceptor Mn-Eu which can further decrease the ECL signals of luminol. These results suggested that the quenching mechanism may be via the synergistic effect between Mn-Eu inhibiting the electrooxidation of H_2O_2 and ECL-RET.

3.3. CV, EIS and ECL measurement of the immunosensor

To verify the stepwise assembly process of the constructed immunosensor, ECL behavior with different stages was performed. As observed in Fig. 4B, compared to bare ITO (curve a), Lu-PtCo-$CuFe_2O_4$-rGO/ITO showed a remarkable ECL signal (curve b). After Ab_1, BSA and procalcitonin successively assembled on Lu-PtCo-$CuFe_2O_4$-rGO/ITO, ECL intensity decreased in sequence (curve c-e). This was because Ab_1, BSA and procalcitonin were belonged to proteins which hindered electron transfer inhibiting ECL reactions. However, after Mn-Eu-Ab_2 attached on the modified-ITO through specific interaction between antibodies and antigens, the ECL signals largely decreased (curve f) which was due to strong quenching effect of Mn-Eu on luminol/H_2O_2 system. These results confirmed that the fabricated process was successful.

EIS and CV were employed to investigate the electrochemical performance of stepwise interfacial modification. As depicted in Fig. 4C, compare to bare ITO (curve a), Lu-PtCo-$CuFe_2O_4$-rGO modified-ITO exhibited a smaller semicircle domain (curve b) and the R_{et} value of Lu-PtCo-$CuFe_2O_4$-rGO decreased slightly (Table S1). This was because the conductivity of ITO sensing interface was improved by Lu-PtCo-$CuFe_2O_4$-rGO with well conductivity. This inference was also confirmed by CV measurement (Fig. 4D) and couple of reversible redox peaks was observed due to the presence of $[Fe(CN)_6]^{3-}$. The current intensity of oxidation peak for Lu-PtCo-$CuFe_2O_4$-rGO/ITO (curve b in Fig. 4D) was higher than bare ITO (curve a in Fig. 4D). After Ab_1, BSA and procalcitonin successive modified on Lu-PtCo-$CuFe_2O_4$-rGO/ITO surface, the semicircle domain and the R_{et} value increased (curve c-e in Fig. 4C) due to Ab_1, BSA and procalcitonin as proteins hindering the electron transfer. After Mn-Eu-Ab_2 attached on procalcitonin/BSA/Ab_1/Lu-PtCo-$CuFe_2O_4$-rGO/ITO surface, the semicircle domain and the R_{et} value further increased (curve f in Fig. 4C), indicating the assembly procedure of ECL immunosensor successful. In CV results, when Ab_1, BSA, procalcitonin and Mn-Eu-Ab_2, immobilized on the modified-ITO, the oxidation peak height decreased successively (curve c-f in Fig. 4D) because of the formation of proteins' layers hindering the electron transfer.

3.4. Optimization of experimental conditions

Optimization of experimental conditions can make the performance of the fabricated ECL immunosensor reach optimal. Four main parameters were optimized, including pH and concentration of H_2O_2, Lu-PtCo-$CuFe_2O_4$-rGO and Mn-Eu. The ECL intensity mainly depended on the pH value of substrate solution. As shown in Fig. S5A, pH values were adjusted from 6.0 to 9.0. When the pH was lower 8.0, the ECL intensity was weak. However, when the pH was 8.0, the ECL intensity increased sharply due to the deprotonation of luminol and when the pH was more than 8.0, the ECL intensity changed gently. The concentration of H_2O_2 could influence producing $O_2^{\cdot-}$ which was the essential species of generating ECL signals. As presented in Fig. S5B, ECL intensity increased with increasing the concentration of H_2O_2 from 1 mM to 6 mM and then decreased gently. Different concentration of Lu-PtCo-$CuFe_2O_4$-rGO could cause different ECL intensity and the reason may be different dosage of Lu-PtCo-$CuFe_2O_4$-rGO on the ITO surface would change the conductivity of modified-ITO platform. When the concentration of Lu-PtCo-$CuFe_2O_4$-rGO increased, the ECL intensity increased (Fig. S5C). When the concentration increased 2.5 mg/mL, ECL intensity reached highest value. Though the concentration further increased, the ECL intensity also decreased because of thick film of Lu-PtCo-$CuFe_2O_4$-rGO hindering the conductivity of sensing interface. To ensure optimal quenching effect, the concentration of Mn-Eu was optimized (Fig. S5D). When the concentration of Mn-Eu was 2 mg/mL, the quenching effect achieved optimal. Therefore, pH 8.0, 6 mM of H_2O_2, 2.5 mg/mL of Lu-

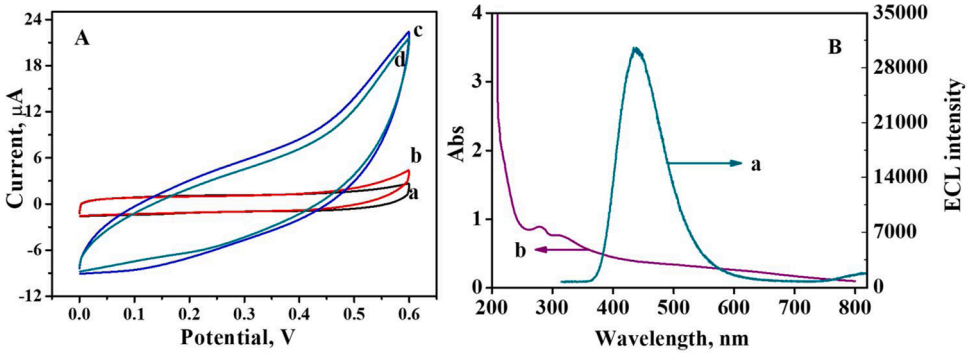

Fig. 3. (A) The CV of bare GCE (a and b), Mn-Eu/GCE (c and d) in the absence and presence of H_2O_2 was performed in 10 mL PBS (pH 8.0) containing 10 μM H_2O_2; (B) ECL emission spectra of luminol (a) and UV–vis absorbance spectra of Mn-Eu (b).

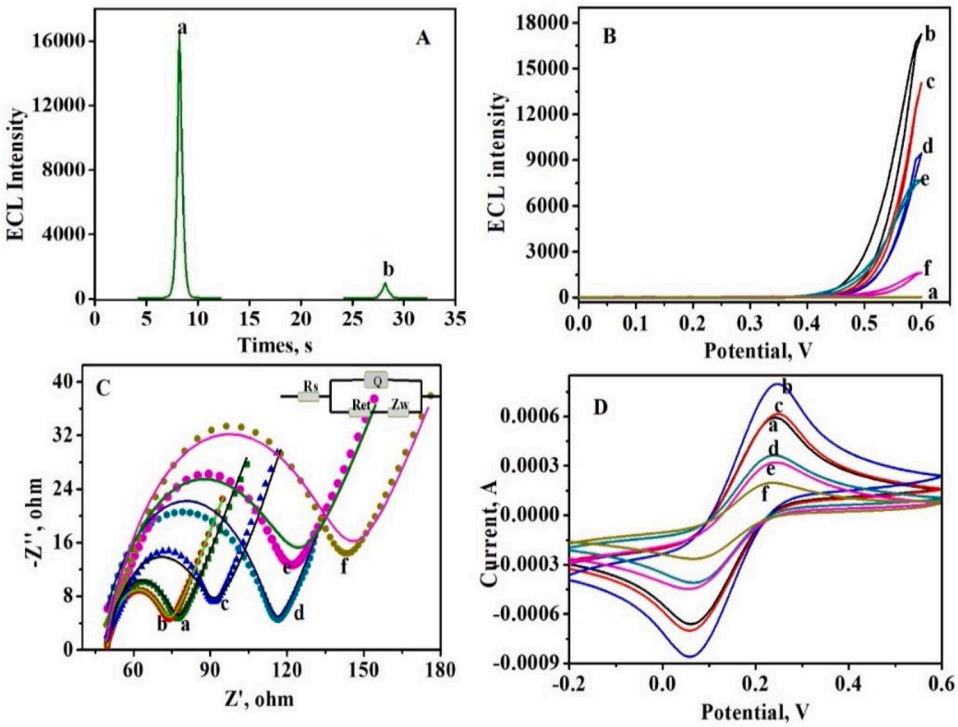

Fig. 4. (A) ECL behavior of Lu-PtCo-$CuFe_2O_4$-rGO/ITO (curve a) and Mn-Eu/Lu-PtCo-$CuFe_2O_4$-rGO/ITO (curve b) in pH 8.0 PBS containing 6 mM H_2O_2; (B) ECL intensity-Potential curves of bare ITO (curve a), Lu-PtCo-$CuFe_2O_4$-rGO/ITO (curve b), Ab_1/Lu-PtCo-$CuFe_2O_4$-rGO/ITO (curve c), BSA/Ab_1/Lu-PtCo-$CuFe_2O_4$-rGO/ITO (curve d), procalcitonin/BSA/Ab_1/Lu-PtCo-$CuFe_2O_4$-rGO/ITO (curve e), and Mn-Eu-Ab_2/procalcitonin/BSA/Ab_1/Lu-PtCo-$CuFe_2O_4$-rGO/ITO (curve f) in pH 8.0 PBS containing 6 mM H_2O_2; (C) EIS of bare ITO (curve a), Lu-PtCo-$CuFe_2O_4$-rGO/ITO (curve b), Ab_1/Lu-PtCo-$CuFe_2O_4$-rGO/ITO (curve c), BSA/Ab_1/Lu-PtCo-$CuFe_2O_4$-rGO/ITO (curve d), procalcitonin/BSA/Ab_1/Lu-PtCo-$CuFe_2O_4$-rGO/ITO (curve e), and Mn-Eu-Ab_2/procalcitonin/BSA/Ab_1/Lu-PtCo-$CuFe_2O_4$-rGO/ITO (curve f) performed in 2.5 mM $[Fe(CN)_6]^{3-/4-}$ and 0.1 M KNO_3; The inset was the equivalent circuit for EIS; (D) CV of bare ITO (curve a), Lu-PtCo-$CuFe_2O_4$-rGO/ITO (curve b), Ab_1/Lu-PtCo-$CuFe_2O_4$-rGO/ITO (curve c), BSA/Ab_1/Lu-PtCo-$CuFe_2O_4$-rGO/ITO (curve d), procalcitonin/BSA/Ab_1/Lu-PtCo-$CuFe_2O_4$-rGO/ITO (curve e), and Mn-Eu-Ab_2/ procalcitonin/BSA/Ab_1/Lu-PtCo-$CuFe_2O_4$-rGO/ITO (curve f) in 5 mM $[Fe(CN)_6]^{3-}$ and 0.1 M KNO_3.

PtCo-$CuFe_2O_4$-rGO and 2 mg/mL of Mn-Eu-Ab_2 were chosen as the optimal conditions for fabricating ECL immunosensor to detect procalcitonin.

3.5. Performance of the immunosensor

Fig. 5A showed the ECL responses with the increment of procalcitonin concentrations. The ECL intensity linearly decreased depending on

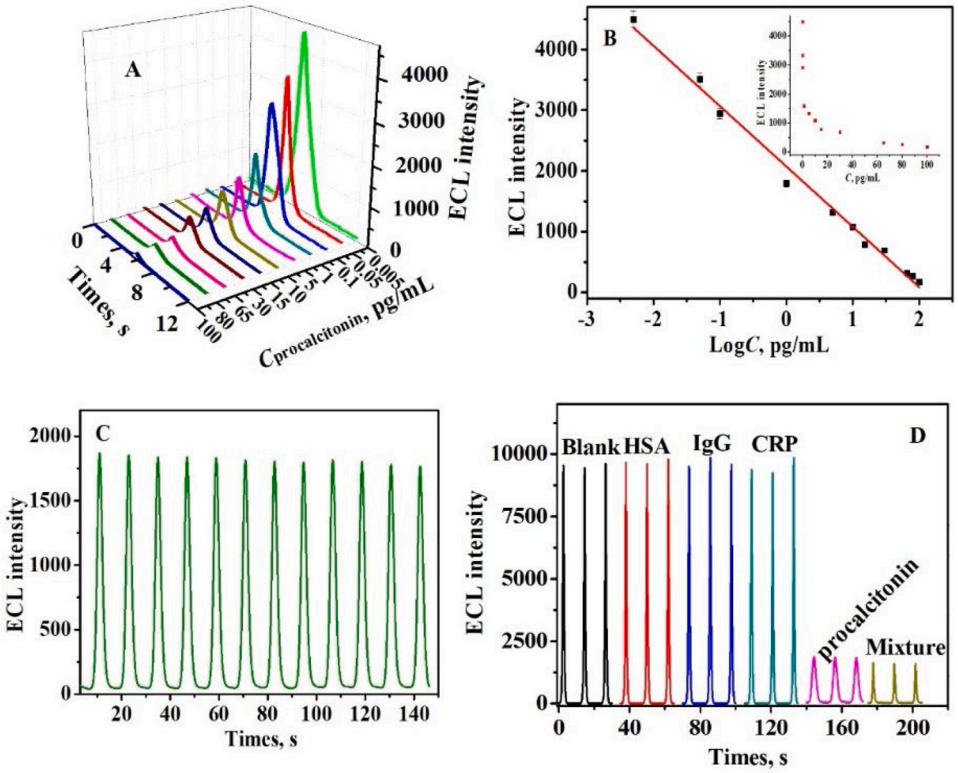

Fig. 5. ECL response of the ECL immunosensor to detect procalcitonin with different concentrations in pH 8.0 PBS containing 6 mM H_2O_2 (A); Linear calibration curve from 0.005 pg/mL to 100 pg/mL. Inset: calibration curve for procalcitonin (B); The stability of ECL immunosensor for the detection of 1 pg/mL under 12 cycles of consecutive cyclic potential scan from 0 to 0.6 V (C); Specificity of the proposed immunosensor (D). Error bars = RSD ($n = 3$).

the logarithm of procalcitonin concentrations in the range from 0.005 pg/mL to 100 pg/mL (Fig. 5B) and the linear regression equation was I=−993.3 log C +2077.5 (unit of C was pg/mL) with the correlation coefficient of 0.9954. The limit of detection (LOD) was calculated according to the previous reports [30]. The calculation procedure of detection limit was as follows: LOD = $3S_B/m$, where m was the slope of the corresponding calibration curve and S_B was the standard deviation of the blank. Herein, the LOD was 0.0021 pg/mL (S/N = 3), and in comparison with other developed immunosensor, this work exhibited lower detection limit and wider linear range (Table S2). This advantage may be ascribed to excellent ECL behavior of substrate materials Lu-PtCo-$CuFe_2O_4$-rGO and well quenching effect of Mn-Eu.

3.6. Stability, selectivity and reproducibility of the signal-off ECL immunosensor

The stability of ECL immunosensor was the foundation of practical application. Therefore, the stability of substrate materials Lu-PtCo-$CuFe_2O_4$-rGO and the immunosensor for detecting 1 pg/mL procalcitonin was investigated. As depicted in Fig. S6, under 20 cycles of consecutive cyclic potential scan, quite stable and strong ECL signals were obtained, indicating PtCo-$CuFe_2O_4$-rGO immobilized luminol exhibiting satisfying ECL behavior. After immunosensor fabricated, Fig. 5C showed the ECL stability of the immunosensor for detecting 1 pg/mL procalcitonin. Under 12 cycles of consecutive cyclic potential scan, the ECL intensity was extremely stable and the Relative Standard Deviation (RSD) was 1.6 %.

The proposed ECL immunosensor was considered to be specific towards detecting procalcitonin based on antigens and antibodies specific recognitions. As presented in Fig. 5D, when interferences Human serum albumin (HSA), Immunoglobulin G (IgG) and C-reactive protein (CPR) were dropped replacing procalcitonin, the ECL intensities were close to the blank samples. After 1 pg/mL procalcitonin and 100 pg/mL interferences HSA, IgG and CPR incubated with the modified ITO, the ECL signals were nearly the same with procalcitonin. These results indicated that excellent selectivity of the proposed immunosensor achieved. Moreover, the reproducibility of the proposed immunosensor was investigated which was shown in Fig. S7. The RSD was 0.79 % for the detection of 1 pg/mL procalcitonin, implying that the immunosensor exhibited well reproducibility. Besides, 5 electrodes of the developed immunosensor was stored at 4 °C for 2 weeks and the storage stability was detected. As shown in Fig. S8, the ECL intensity was maintained 88.5 % of its original ECL intensity, suggesting that the immunosensor held satisfying storage stability.

3.7. The application of the developed ECL immunosensor in human serum

In order to study the potential feasibility of the developed ECL immunosensor in human serum, different concentrations of procalcitonin were evaluated through standard addition method. As shown in Table S3, satisfying recoveries and RSD were displayed, indicating that the developed immunosensor could be used as an effective tool to detect procalcitonin in human serum.

4. Conclusion

In this work, PtCo-$CuFe_2O_4$-rGO was synthesized to combine with luminol through electrostatic attraction which possessing excellent ECL signals. This was because PtCo and $CuFe_2O_4$ nanoparticles can facilitate the decomposition of H_2O_2 producing more ROS and increase the electrooxidation of H_2O_2. And Lu-PtCo-$CuFe_2O_4$-rGO was employed to construct a sandwich immunosensor to detect procalcitonin based on Mn-Eu labeled Ab_2 to quench the ECL behavior of luminol/H_2O_2 system. Herein, the end potential of the applied potential was at 0.6 V which satisfied the detecting need and lower potential can ensure the activity of biomolecules. The quenching mechanism could be due to Mn-Eu as antioxidant suppressing the electrooxidation of H_2O_2 and the existence of ECL-RET between luminol and Mn-Eu. The analysis of results indicated that the developed ECL immunosensor displayed well analytical performance according to sensitivity, stability, selectivity and reproducibility.

CRediT authorship contribution statement

Xiaojian Li: Conceptualization, Data curation, Writing - original draft. **Yu Du:** Methodology, Writing - review & editing. **Yueyun Li:** Formal analysis. **Xiang Ren:** Formal analysis. **Hongmin Ma:** Methodology, Writing - review & editing. **Huan Wang:** Methodology. **Qin Wei:** Funding acquisition, Project administration. **Huangxian Ju:** Formal analysis.

Declaration of Competing Interest

The authors declare that they have no known competing financial interests or personal relationships that could have appeared to influence the work reported in this paper.

Acknowledgements

This study was supported by the National Key Scientific Instrument and Equipment Development Project of China (No. 21627809) and National Natural Science Foundation of China (Nos. 21575050 and 21777056).

Appendix A. Supplementary data

Supplementary material related to this article can be found, in the online version, at doi:https://doi.org/10.1016/j.snb.2020.128702.

References

[1] J.E. Dick, C. Renault, B.-K. Kim, A.J. Bard, Electrogenerated chemiluminescence of common organic luminophores in water using an emulsion system, J. Am. Chem. Soc. 136 (2014) 13546–13549.
[2] X. Qin, Y. Dong, M. Wang, Z. Zhu, M. Li, D. Yang, et al., In situ growing triethanolamine-functionalized metal–organic frameworks on two-dimensional carbon nanosheets for electrochemiluminescent immunoassay, ACS Sens. 4 (2019) 2351–2357.
[3] Y. Cao, Z. Zhang, L. Li, J.-r. Zhang, J.-J. Zhu, An improved strategy for high-quality cesium bismuth bromine perovskite quantum dots with remarkable electrochemiluminescence activities, Anal. Chem. 91 (2019) 8607–8614.
[4] J. Jiang, D. Chen, X. Du, Ratiometric electrochemiluminescence sensing platform for sensitive glucose detection based on in situ generation and conversion of coreactants, Sens. Actuators B Chem. 251 (2017) 256–263.
[5] H.R. Zhang, M.-S. Wu, J.-J. Xu, H.-Y. Chen, Signal-on dual-potential electrochemiluminescence based on luminol–gold bifunctional nanoparticles for telomerase detection, Anal. Chem. 86 (2014) 3834–3840.
[6] C. Karthikeyan, R.K.S. Sheet, D.J. Yoo, Y.S. Lee, S.K. Yesupatham, et al., Pigeon excreta mediated synthesis of rGO/$CuFe_2O_4$ nanocomposite and its catalytic activity toward sensitive and selective hydrogen peroxide detection, ACS Sustainable Chem. Eng. 5 (2017) 4897–4905.
[7] J. Gao, S. Wu, Y. Han, F. Tan, Y. Shi, M. Liu, et al., 3D mesoporous $CuFe_2O_4$ as a catalyst for photo-fenton removal of sulfonamide antibiotics at near neutral pH, J. Colloid Interface Sci. 514 (2018) 409–416.
[8] S. Fan, X. Li, L. Zeng, M. Zhang, Z. Yin, T. Lian, et al., Relationships between crystal, internal microstructures, and physicochemical properties of copper–zinc–iron multinary spinel hierarchical nano-microspheres, ACS Appl. Mater. Interfaces 10 (2018) 35919–35931.
[9] Y. Liu, Z. Guo, F. Li, Y. Xiao, Y. Zhang, T. Bu, et al., Multifunctional magnetic copper ferrite nanoparticles as fenton-like reaction and near-infrared photothermal agents for synergetic antibacterial therapy, ACS Appl. Mater. Interfaces 11 (2019) 31649–31660.
[10] W. Zhang, B. Quan, C. Lee, S.-K. Park, X. Li, E. Choi, et al., One-step facile solvothermal synthesis of copper ferrite–graphene composite as a high-performance supercapacitor material, ACS Appl. Mater. Interfaces 7 (2015) 2404–2414.
[11] J. Li, H. Jiang, X. Rao, Z. Liu, H. Zhu, Y. Xu, Point-of-Care testing of pathogenic Bacteria at the single-colony level via gas pressure readout using aptamer-coated magnetic CuFe2O4 and vancomycin-capped platinum nanoparticles, Anal. Chem. 91 (2018) 1494–1500.

[12] B. Haghighi, A. Tavakoli, S. Bozorgzadeh, Improved electrogenerated chemiluminescence of luminol by cobalt nanoparticles decorated multi-walled carbon nanotubes, J. Electroanal. Chem. Lausanne (Lausanne) 762 (2016) 80–86.
[13] S.D. Carrigan, S. George, T. Maryam, Toward resolving the challenges of sepsis diagnosis, Clin. Chem. 50 (2004) 1301–1314.
[14] H. Li, Y. Sun, J. Elseviers, S. Muyldermans, S. Liu, Y. Wan, A nanobody-based electrochemiluminescent immunosensor for sensitive detection of human procalcitonin, Analyst 139 (2014) 3718–3721.
[15] S. Liliana, G. France, D.K. Amre, S.L. Patrick, L. Jacques, Serum procalcitonin and C-reactive protein levels as markers of bacterial infection: a systematic review and meta-analysis, Clin. Infect. Dis. 39 (2004) 206–217.
[16] N. Mancini, S. Carletti, N. Ghidoli, P. Cichero, R. Burioni, M. Clementi, The era of molecular and other non-culture-based methods in diagnosis of sepsis, Clin. Microbiol. Rev. 23 (2010) 235–251.
[17] M. d'Ischia, A. Napolitano, V. Ball, C.-T. Chen, M.J. Buehler, Polydopamine and eumelanin: from structure–property relationships to a unified tailoring strategy, Acc. Chem. Res. 47 (2014) 3541–3550.
[18] K.A. Yan Chen, Jianhu Liu, Xiaoyan Ren, Chunhuan Jiang, Lehui Lu, Polydopamine-based coordination nanocomplex for T1/T2 dual mode magnetic resonance imaging-guided chemo-photothermal synergistic therapy, Biomaterials 77 (2016) 198–206.
[19] S. Cho, W. Park, D.-H. Kim, Silica-coated metal chelating-melanin nanoparticles as a dual-modal contrast enhancement imaging and therapeutic agent, ACS Appl. Mater. Interfaces 9 (2016) 101–111.
[20] W. Xu, J. Sun, L. Li, X. Peng, R. Zhang, B. Wang, Melanin-manganese nanoparticles with ultrahigh efficient clearance in vivo for tumor-targeting T1 magnetic resonance imaging contrast agent, Biomater. Sci. 6 (2018) 207–215.
[21] A. Pezzella, A. Iadonisi, S. Valerio, L. Panzella, A. Napolitano, M. Adinolfi, et al., Disentangling eumelanin "Black chromophore": visible absorption changes As signatures of oxidation state- and aggregation-dependent dynamic interactions in a model water-soluble 5,6-Dihydroxyindole polymer, J. Am. Chem. Soc. 131 (2009) 15270–15275.
[22] A.B. Mostert, G.R. Hanson, T. Sarna, I.R. Gentle, B.J. Powell, P. Meredith, Hydration-controlled X-Band EPR spectroscopy: a tool for unravelling the complexities of the solid-state free radical in eumelanin, J. Phys. Chem. B 117 (2013) 4965–4972.
[23] M. Gauden, A. Pezzella, L. Panzella, M.T. Neves-Petersen, E. Skovsen, S.B. Petersen, et al., Role of solvent, pH, and molecular size in excited-state deactivation of key eumelanin building blocks: implications for melanin pigment photostability, J. Am. Chem. Soc. 130 (2008) 17038–17043.
[24] A.B. Mostert, B.J. Powell, F.L. Pratt, G.R. Hanson, T. Sarna, I.R. Gentle, et al., Role of Semiconductivity and ion transport in the electrical conduction of melanin, Proc. Natl. Acad. Sci. U. S. A 109 (2012) 8943–8947.
[25] H. Liu, C. Chu, Y. Liu, X. Pang, Y. Wu, Z. Zhou, et al., Novel intrapolymerization doped manganese-eumelanin coordination nanocomposites with ultrahigh relaxivity and their application in tumor theranostics, J. Adv. Sci. 5 (2018) 1800032–11800040.
[26] Y. Liu, W. Zhen, L. Jin, S. Zhang, H. Zhang, All-in-one theranostic nanoagent with enhanced reactive oxygen species generation and modulating tumor microenvironment ability for effective tumor eradication, ACS Nano 12 (2018) 8943–8947.
[27] H. Wang, S. Bai, Y. Pi, Q. Shao, Y. Tan, X. Huang, A strongly coupled ultrasmall Pt_3Co nanoparticle-ultrathin $Co(OH)_2$ nanosheet architecture enhances selective hydrogenation of α,β-unsaturated aldehydes, ACS Catal. 9 (2019) 154–159.
[28] X. Yu, X. An, A. Genç, M. Ibáñez, A. Cabot, Cu_2ZnSnS_4-PtM (M = Co, Ni) nanoheterostructures for photocatalytic hydrogen evolution, J. Phys. Chem. C 119 (2015) 21882–21888.
[29] A. Escobar, L. Yate, M. Grzelczak, H. Amenitsch, P.C. Angelomé, One-step synthesis of mesoporous silica thin films containing available COOH groups, ACS Omega 2 (2017) 4548–4555.
[30] X. Li, X. Sun, D. Fan, T. Yan, R. Feng, H. Wang, et al., A ternary quenching electrochemiluminescence insulin immunosensor based on Mn^{2+} released from MnO_2 carbon core-shell nanospheres with ascorbic acid quenching AuPdPt–MoS_2@TiO_2 enhanced luminol, Biosens. Bioelectron. 142 (2019) 111551–111557.

Xiaojian Li studies in school of chemistry and chemical engineering, University of Jinan as doctoral student.

Yu Du works and studies in School of Chemistry and Chemical Engineering, University of Jinan as a teacher. Her main research interests are the determination of electrochemiluminescence immunosensor.

Peng Xu studies in school of chemistry and chemical engineering, University of Jinan as postgraduate student.

Yueyun Li received her M.S. degree in applied chemistry from Nanjing Tech University in 2002 and Ph.D. degree in analytical chemistry from China University of Geosciences in 2018. Now, she is a professor at Shandong University of Technology. Her main research interests are electrochemical biosensors and photoelectrochemical biosensors and has published many articles on analysis, immunosensor and applied successfully for many research projects, such as Biosens. Bioelectron., Sens. Actuators B: Chem et al.

Xiang Ren received his B.S. degrees in Chemistry of Materials/English from University of Jinan in 2012, M.S. degree in Chemical Engineering and Technology from University of Jinan in 2015, and Ph.D. degree from University of Jinan/University of Electronic Science and Technology of China in 2019. Now, he is an associate professor in University of Jinan. His main research interests are energy catalysis, nanomaterials controlled-synthesis, and electrochemical biosensors.

Huan Wang received Ph.D. degree from China university of Geosciences (Beijing). Now, he is an associate professor at University of Jinan. His main research interests are the determination of electrochemical immunosensor.

Hongmin Ma received both his B.S. and M.S. degree in Applied Chemistry from University of Jinan in 2005 and 2008 respectively. And he has received his Ph.D. degree in Colloid and Interface Chemistry at Shandong University, investigating self-assembly at all scales at surfaces in 2011. Now, he is a professor at University of Jinan, interested in the assembly of nano-composites and the construction of ordered porous films as well as their analytical applications.

Qin Wei, a professor and DSc, has devoted herself to analytical teaching and scientific research. Her main research interests are the determination of protein and nucleic acid by photometry and the electrochemical immunosensor preparation. She has published over one hundred articles on analysis, immunosensor and applied successfully for many research projects, such as *Biomaterials, Adv. Funct. Mater., Biosens. Bioelectron., Sens. Actuators B: Chem., Talanta.*

Huangxian Ju received his BS, MS and Ph.D. degrees from Nanjing University during 1982–1992. He was a postdoc in Montreal University (Canada) from 1996 to 1997 and a guest professor in three universities of Germany and Ireland in 1999−2000. He became an associate and full professor of Nanjing University in 1993 and 1999. He is currently the director of State Key Laboratory of Analytical Chemistry for Life Science. His research interests focus on analytical biochemistry, biosensing and molecular diagnosis. He has published 616 papers in different journals with SCI h-index of 83 (29,523 citations) and Google Scholar h-index of 91 with more than 29,000 citations.